Received: 14 October 2017 | Revised: 28 December 2017 | Accepted: 29 December 2017

DOI: 10.1002/aoc.4291

FULL PAPER

WILEY Applied Organometallic Chemistry

Ultrasonic and bio-assisted synthesis of Ag@HNTs-T as a novel heterogeneous catalyst for the green synthesis of propargylamines: A combination of experimental and computational study

Masoumeh Malmir[1] | Majid M. Heravi[1] | Samahe Sadjadi[2] | Tayebeh Hosseinnejad[1]

[1] Department of Chemistry, School of Science, Alzahra University, PO Box 1993891176 Vanak, Tehran, Iran

[2] Gas Conversion Department, Faculty of Petrochemicals, Iran Polymer and Petrochemicals Institute, PO Box 14975-112, Tehran, Iran

Correspondence
Majid M. Heravi, Department of Chemistry, School of Science, Alzahra University, Vanak, Tehran, Iran, PO Box 1993891176.
Email: mmh1331@yahoo.com; mmheravi@alzahra.ac.ir

A novel heterogeneous catalyst is prepared through functionalization of halloysite nanotube with 1*H*-1,2,3-triazole-5-methanol and subsequent immobilization of silver nanoparticles through bio-assisted approach using Arctiumplatylepis extract. The resulting catalyst, Ag@HNTs-T, was characterized by using SEM/EDX, BET, XRD, FTIR, ICP-AES, TGA, DTGA and elemental mapping analysis. Moreover, we computationally assessed metal-ligand interactions in Ag@HNTs-T complex model to interpret the immobilization behavior of silver nanoparticles on HNTs surface *via* quantum chemistry computations. The catalytic activity of the catalyst was studied for the synthesis of propargylamines *via* A^3 and KA^2 coupling reactions under ultrasonic irradiation. The results demonstrated that Ag@HNTs-T could efficiently promote these reactions to furnish the corresponding products in high yields and short reaction times. The study of the recyclability of the catalyst and Ag(0) leaching confirmed that the catalyst was recyclability up to four reaction runs with slight Ag(0) leaching.

KEYWORDS
A^3 and KA^2 coupling reactions, bio-synthesis, DFT and PCM calculations, halloysite, silver nanoparticles

1 | INTRODUCTION

A^3 and KA^2 coupling reactions are three-component reactions of amines, acetylenes and aldehydes or ketones respectively. These reactions precede through activation of terminal alkyne C–H bond in the presence of a catalyst such as Ni, Cu, Ir, Ag, Cu, Fe and Au-based catalysts,[1–6] followed by reaction with carbonyl and amine compounds and lead to the formation of propargylamines, which are important synthetic versatile intermediates with utility for the preparation of complicated heterocycles and natural products.[1,7] Although these reactions are superior to many previously reported protocols[1,8,9] for the synthesis of propargylamines, some issues such as using toxic solvents, costly catalysts and reaction media, have been still unsolved.

Halloysite nanotubes, HNTs, is a naturally occurring phyllosilicate with Al: Si ratio of 1:1, similar to the platy kaolinite and general formula of $(Al_2(OH)_4Si_2O_5.2H_2O)$. Pristine HNTs, which can be found in regions such as china, USA, France and New Zealand in large scale, [10] has tubular morphology with the external diameters varying between 30 to 190 nm, internal diameters ranging between 10-100 nm and length of about 100 nm to 4000 nm.[11,12] Recently, the use of HNTs in various research fields including catalysis and photo

catalysis,[13,14] waste treatment, polymeric matrices, separation technology,[15] drug delivery,[13] nanomaterial and optical, magnetic and electrical applications[16] has been rapidly increased. Between several applications, the utility of HNTs as a support for immobilization of the catalytic species gained growing attention.[11] Recently, Riela, Lazzara et al. have published an excellent review article [10] on the use of HNT as a support for developing metal-based catalysts. In recent advances in this topic, surface functionalization of HNTs has been introduced as a potent way to manipulate the properties of HNTs and improve the immobilization of the catalytic species such as metal nanoparticles.[10,17–22]

Following our attempt for disclosing efficient and eco-friendly protocols for the synthesis of chemicals through applying novel heterogeneous catalysts,[23–25] we have recently focused our attention on the functionalization of HNTs with various functionalization agents and studying the utility of functionalized HNTs as efficient support for immobilization of catalytically active species such as heteropolyacid[26,27] and ionic liquids.[28] The results of our researches as well as other research groups[10] clearly established that the functionality on the surface of HNTs has a significant role in efficient immobilization and suppressing the leaching of the catalytic species. To shed more light to the interactions of HNT and the catalytic species, we also exploited theoretical chemistry[29] and proved that the number and nature of the heteroatoms on the functionality crucially affect the interaction of catalytic species with HNTs.

Based on our focus on combined experimental and computational design of heterogeneous nanocatalysts and their applications in organic reactions,[30,31] we have recently analysed and reported metal-ligand interactions between metal nanoparticles and several amine functionalized polymeric and silica bonded mesoporous supports from the structural, electronic and thermochemical viewpoints.[32–41] Regarding the importance of information about the physicochemical properties of support surfaces in their computational design and applications,[42–45] in this research we investigated computationally the immobilization behaviour of silver nanoparticles on 1*H*-1,2,3-triazole-5-methanol functionalized HNTs surface. For being more astute, we assessed metal-ligand interactions in 1*H*-1,2,3-triazole-5-methanol functionalized HNTs silver complex model (Ag@HNTs-T) using density functional theory (DFT)[46] and polarized continuum (PCM)[47] methods and more importantly we employed our calculated results to interpret some of our experimental elucidations.

Motivated by the excellent catalytic performance of HNTs and in attempt to further disclose the interactions of HNT and the catalytically active species, herein, we report design and synthesis of a novel catalyst, in which HNTs was functionalized with 1*H*-1,2,3-triazole-5-methanol and used as a support for the immobilization of bio-reduced silver nanoparticles. The catalytic activity of the novel catalyst, Ag@HNTs-T, was studied for promoting A^3 and KA^2 coupling reactions *via* a green protocol, i.e., using ultrasonic irradiations in aqueous media (Scheme 1). The recyclability of Ag@HNTs-T and Ag(0) leaching were also studied.

2 | EXPERIMENTAL

2.1 | Materials

Reagents and chemicals used for the synthesis of the catalyst and investigation of its catalytic activity included aliphatic and aromatic aldehydes, cyclic ketone, amines, acetylenes, sodium azide, 3-chloropropyltriethoxysilane, $AgNO_3$, HNTs, toluene, EtOH, chloroform and 1*H*-1,2,3-triazole-5-methanol. The latter was provided from china and other chemicals were purchased from Sigma-Aldrich.

The as-prepared catalyst was successfully characterized by using various characterization techniques including FTIR, XRD, SEM/EDX, TGA, DTGA, ICP-AES and BET. The FTIR spectra were recorded by using PERKIN-ELMER- Spectrum 65 instrument. Room temperature powder X-ray diffraction patterns were obtained by using a Siemens, D5000. CuKα radiation from a sealed tube. SEM/EDX images were provided by applying a Tescan instrument, using Au-coated samples and acceleration voltage of 20 kV. The BET analyses were achieved by BELSORP Mini II instrument. Prior to BET analyses, the catalyst and pristine HNTs were degassed at 423 K for 3 h. All organic products were known and identified by

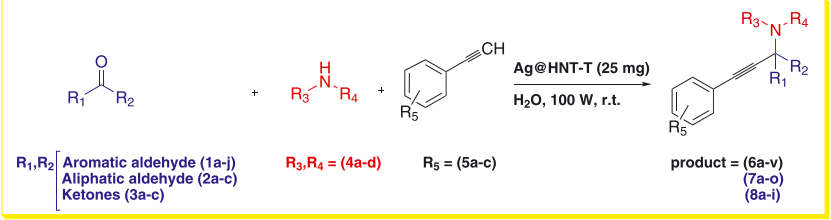

SCHEME 1 A^3 and KA^2 coupling reactions

comparing their melting points (measured by using the capillary tube method with an electro thermal 9200 apparatus) and FTIR spectra with authentic propargylamines. For some selected propargylamines, ^{1}HNMR and ^{13}CNMR spectra were also provided to prove the formation of the desired products.

2.2 | Synthesis of Cl-functionalized HNTs: HNTs-Cl (1)

To prepare HNTs-Cl, 4 ml of 3-chloropropyltriethoxysilane and 1.2 g of HNTs were mixed in 50 ml dry toluene. Then, the obtained mixture was sonicated and homogenized under ultrasonic irradiation of power 100 W. After half an hour, the mixture was heated under reflux condition at 110 °C overnight. Finally, the cream solid was filtered off, washed for three times with dried toluene and dried at 100 °C overnight.

2.3 | Incorporation of 1*H*-1,2,3-triazole-5-methanol: Synthesis of HNTs-T (2)

To synthesis HNTs-T,1*H*-1,2,3-triazole-5-methanol (0.5 g) was introduced to a suspension of HNTs-Cl (1 g in 50 ml dried toluene) and reacted under reflux condition at 110 °C overnight. Upon completion of the reaction, the cream product **2** was filtered, washed with dry toluene three times and dried at 100 °C in oven overnight.

2.4 | Preparation of Arctiumplatylepis flowering plant extracts (3)

Generally, the leaves of Arctiumplatylepis were collected from Tehran city, Iran. First, the violet flower of Arctiumplatylepis was washed with distilled water and crushed in porcelain mortar into powder. The aqueous Arctiumplatylepis extract was prepared by boiling 2 g of powder with 100 ml distilled water for 60 min. The extract

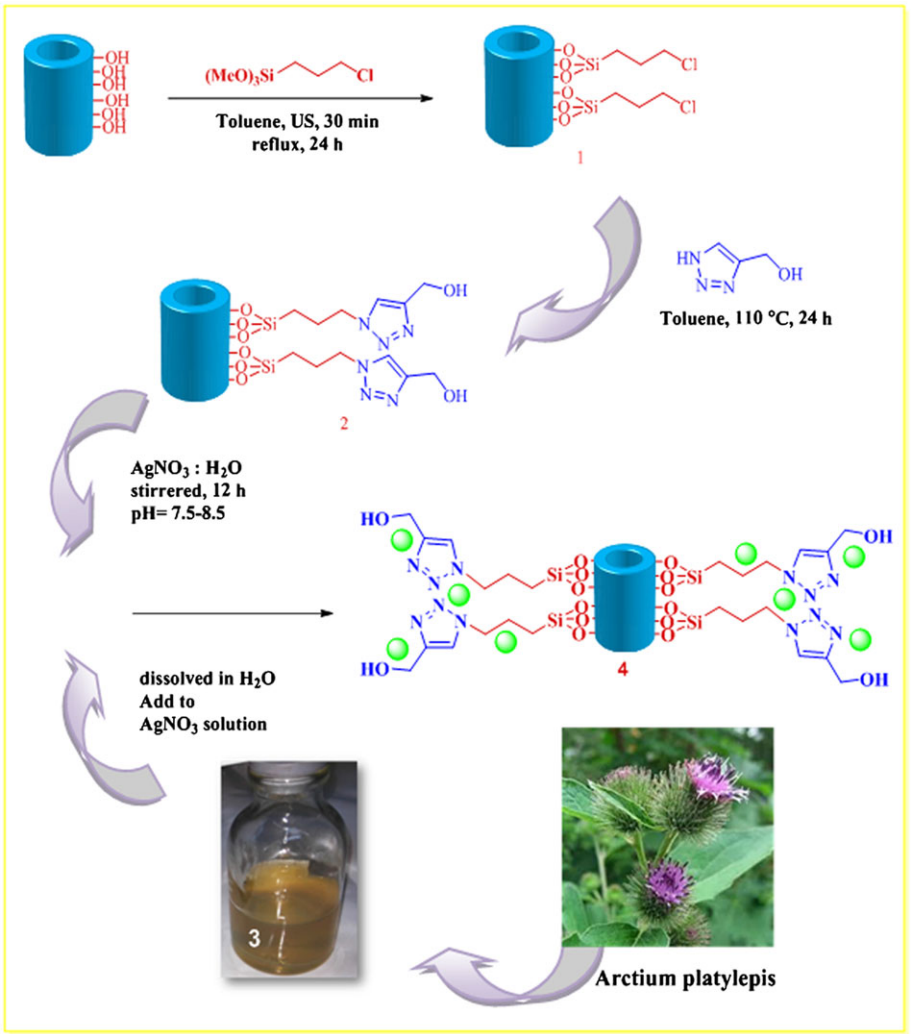

FIGURE 1 Preparation of Ag@HNTs-T catalyst

was cooled to room temperature and filtered through filter paper. Then, the filtrate was collected and the extract **3** was used for the reduction of silver salt and synthesis of Ag NPs.

2.5 | Reduction of Ag(II) to Ag(0) and Loading of Ag nanoparticles on HNTs-T: Synthesis of Ag@HNTs-T (4)

Synthesis and immobilization of Ag nanoparticles were carried out through reaction of HNTs-T (1 g) and aqueous solution of $AgNO_3$ (0.1 gin 20 ml of water) under vigorous stirring at room temperature for 0.5 h followed by reduction of silver salt to the Ag(0) nanoparticles by using the Arctiumplatylepis extract as a reducing and stabilizing agent. In a typical procedure, the fresh extract (2 ml) was dissolved in 20 mL water and then added into the as-prepared mixture of HNTs-T and $AgNO_3$ under stirring. After 12 h, the product **4** was collected, washed with $EtOH/H_2O$ for three times and dried at 60 °C for 12 h. The general synthetic procedure of Ag@HNTs-T is illustrated in Figure 1.

2.6 | Typical Procedure of A^3 and KA^2 Coupling Reactions

In the solution of aldehyde or ketone (1 mmol), alkyne (1.1 mmol) and amine (1 mmol) in water (20 ml) as solvent, 25 mg of Ag@HNTs-T was added. The reaction mixture was then sonicated for appropriate reaction time at 100 W and room temperature. After completion of the reaction (monitored by TLC), the reaction mixture was diluted with hot EtOH (15 ml) and the catalyst was filtered off. The filtrate was then cooled to room temperature to allow the products to precipitate. Finally,

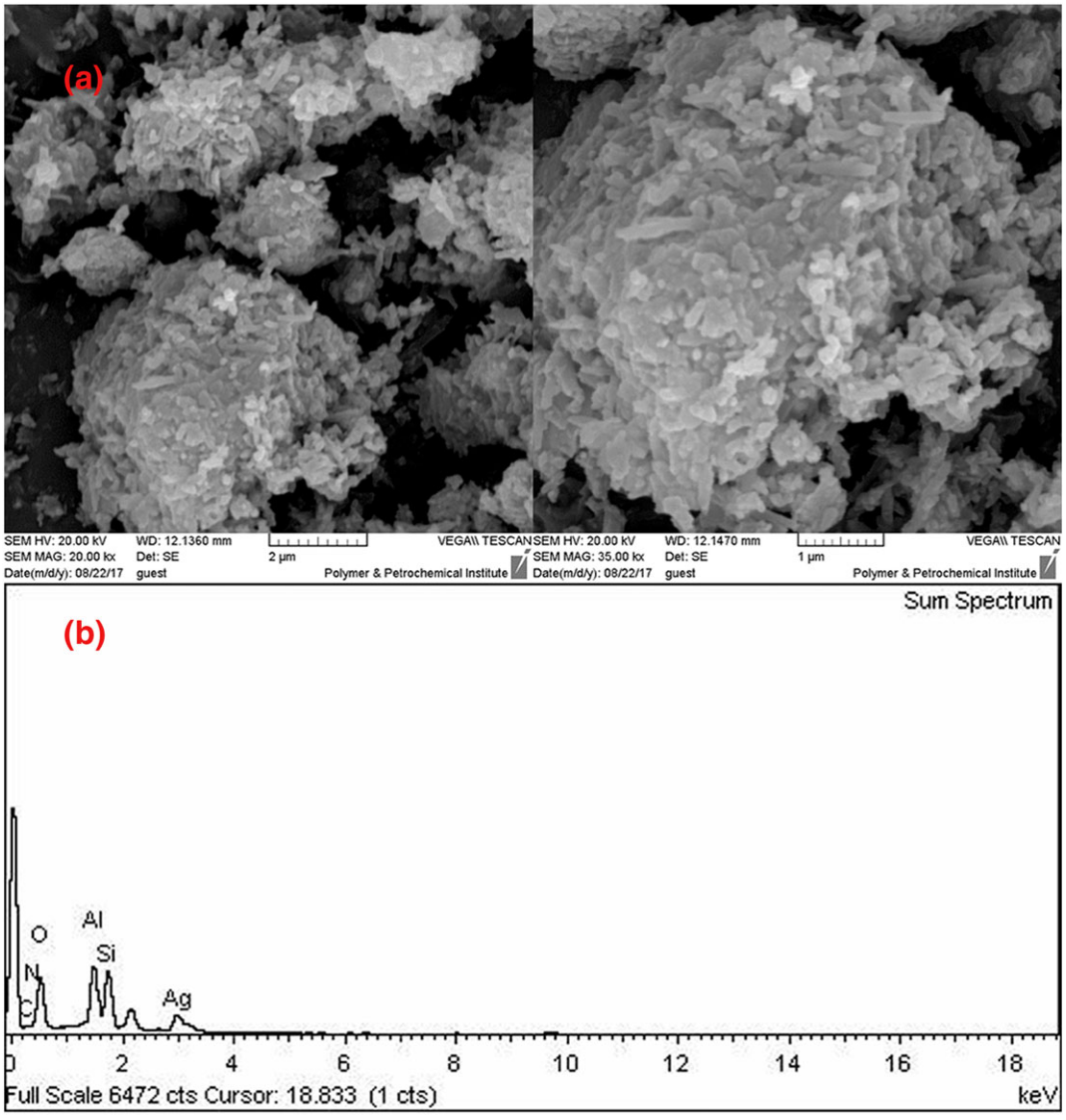

FIGURE 2 The SEM images of Ag@HNTs-T (A) and EDX image of Ag@HNTs-T (B)

the pure products were furnished by re-crystallization with EtOH.

3 | RESULT AND DISCUSSION

3.1 | Characterization of Ag@HNTs-T catalyst

The morphology of the catalyst was studied by using SEM analysis, Figure 2. It can be seen that the final catalyst preserved the tubular morphology of the HNTs. However, the short tubes packed together to form aggregates. The compact morphology of the catalyst can be assigned to the presence of the electrostatic interactions between the organic functionalities and silver nanoparticles which can get the particles closer and form the aggregates.

The EDX images of the Ag@HNTs-T, Figure 2, clearly exhibited the presence of Al, Si and O atoms which can be representative of HNTs framework. Moreover, C and N atoms, which can be attributed to the organic moiety of the catalyst, are present in the EDX analysis. The immobilization of silver nanoparticles can also be confirmed by observation of Ag in EDX analysis.

To study the dispersion of Ag(0) nanoparticles on the functionalized HNTs, elemental mapping analysis of Ag@HNTs-T was performed, Figure 3. As depicted in Figure 3, silver nanoparticles are dispersed on the HNTs-T almost uniformly. Notably, C and N atoms exhibited good dispersion, indicating that the surface of HNTs was uniformly functionalized with organic moiety.

The XRD pattern of the catalyst is depicted in Figure 4 . As shown, the XRD pattern exhibited the characteristic peaks of both Ag nanoparticles and HNT structure, Figure 4. The peaks denoted as star are the characteristic peaks of silver nanoparticle (JCPDS card no. 04-0783) and the speaks labeled as circle (at $2\theta = 8°$, 13°, 23°, 28°, 31°, 58° and 67°) are indicative of HNTs structure (JCPDS No. 29-1487). [11,48] This observation confirmed that HNTs structure is preserved in Ag@HNTs-T. Considering the similarity of interlayer distances of pristine HNTs and

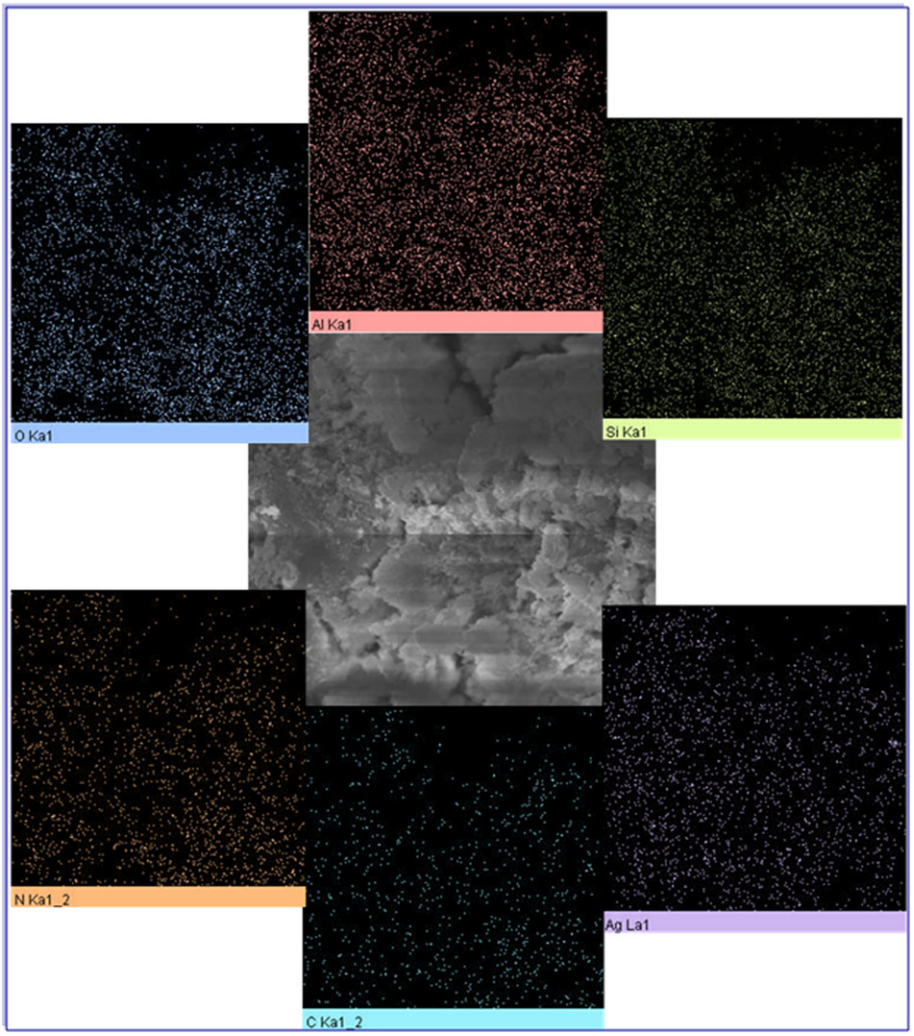

FIGURE 3 The elemental mapping analysis of the Ag@HNTs-T

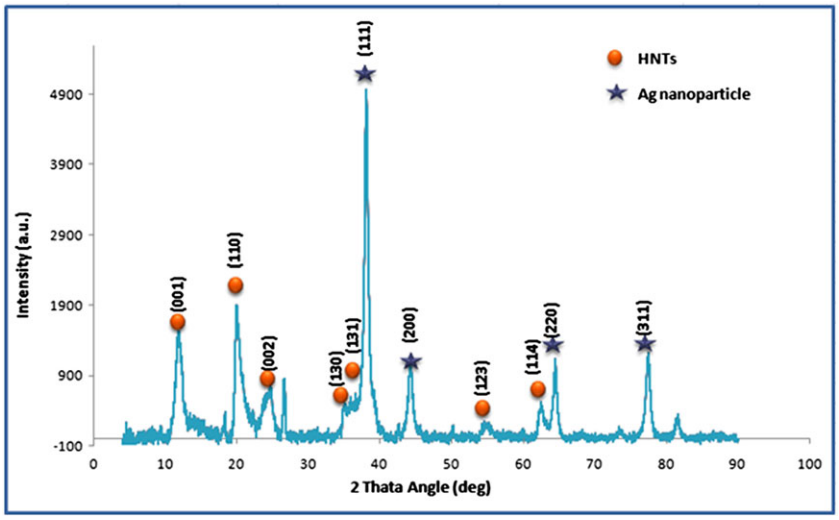

FIGURE 4 The XRD pattern of Ag@HNTs-T

Ag@HNTs-T, it can be concluded that the silver nanoparticles were placed on the surface and the edges of the HNTs tubes. This is in good agreement with previous reports.[11]

To further confirm the formation of the catalyst, FTIR spectra of pristine HNTs, Ag@HNTs-T and HNTs-T were recorded and compared, Figure 5. As depicted in Figure 5 the FTIR spectra are almost similar and in three of them the characteristic bands of HNT, i.e. the bands at 3692 cm^{-1} and 3618 cm^{-1}, which are representative of internal hydroxyl groups of HNTs and the band at 672 cm^{-1} 1029 cm^{-1} that are indicative of Al-O-Si vibration and Si–O stretching as well as the band at 1620 cm^{-1} (the bending of OH groups on interstitial water) and 2905 cm^{-1} can be observed. In the FTIR spectra of Ag@HNTs-T and HNTs-T, the characteristic bands of the organic functionalities, i.e. the band at 2905 cm^{-1} which can be assigned to the $-CH_2$ stretching and the band at 1620 cm^{-1} which can be assigned to the C=N overlapped with the characteristic bands of HNT are clearly observable. In addition to the FTIR data, incorporating of organic functionalities were confirmed by using other characterization methods such as EDX.

To calculate the content of Ag(0) nanoparticles in the catalyst, ICP-AES analysis was applied. Prior to the analysis, the digestion of Ag@HNTs-T was accomplished by using concentrated HCl and HNO_3 solution. ICP-AES analysis of the resulting extract established that the content of silver nanoparticles was 5 %w/w.

Nitrogen adsorption–desorption isotherm of Ag@HNTs-T is illustrated in Figure 6. As depicted, the shape of the isotherm of Ag@HNTs-T is of type II nitrogen adsorption–desorption isotherm with H3 hysteresis loops,[11,27] indicating the porous entity of the catalyst. To provide more insight into the textural properties of the catalyst and elucidate how functionalization of HNTs

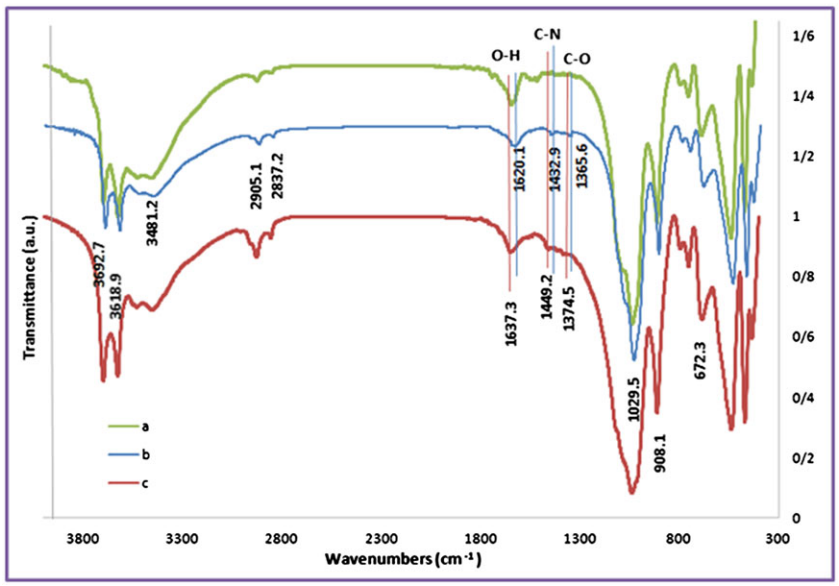

FIGURE 5 The FTIR spectrum of pristine HNTs (a), Ag@HNTs-T catalyst (b) and HNTs-T (c)

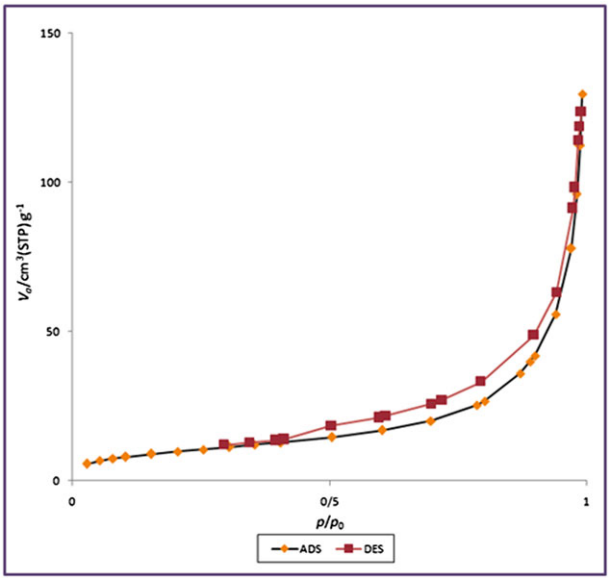

FIGURE 6 N_2 adsorption-desorption isotherms of Ag@HNTs-T

with 1*H*-1,2,3-triazole-5-methanol and immobilization of silver nanoparticles affect the textural features of pristine HNTs, total pore volume, average pore diameter and surface area of the catalyst were compared with those of pristine HNTs, Table 1. As tabulated in Table 1, upon functionalization of HNTs and incorporation of Ag(0) nanoparticles, the surface area decreased compared to pristine HNTs while, the average pore diameter increased. Furthermore, the total pore volume slightly reduced. According to the previous reports, the decrease in the surface area can be attributed to the surface functionalization of HNTs.[27]

Ag@HNTs-T was also subjected to TGA and DTGA analyses. The results of thermal analysis over the range of 35-550 °C, Figure 7, demonstrated that two main degradation occurred over this range. First, the degradation about 200 °C, which can be due to loss of water and second one, about 450 °C, which can be assigned to the loss of organic functional group. Notably, the content of the functionality was estimated to be about 10 % w/w.

3.2 | Computational section

As it was discussed earlier, we have recently focused on the joint experimental and computational assessment of heterogeneous catalysts including modified poly (styrene-co-maleic anhydride) palladium and copper

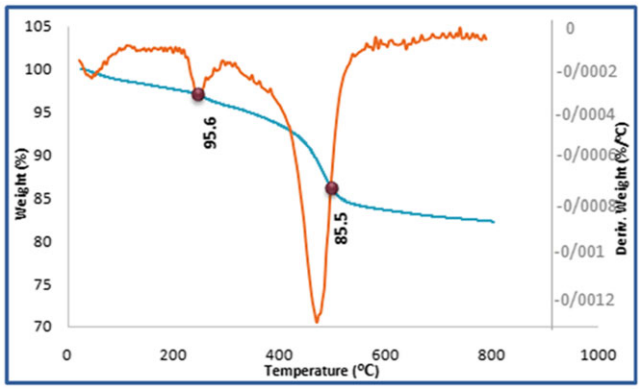

FIGURE 7 The TGA (a) and DTGA (b) analysis of Ag@HNTs

nanocatalyst,[32–35] copper (I) and (II) -aminated KIT-5[37,40] and N-sulfamic-aminated KIT-5 catalysts.[39] Armed with these experiences, we present a quantitative model for description of immobilization behavior of Ag NPs on functionalized HNTs support via DFT[46,49] and PCM[47] computational approaches.

In this content, metal-ligand interactions in 1*H*-1,2,3-triazole-5-methanol functionalized HNTs-supported Ag complex (denoted as Ag@HNTs-T) was investigated from the structural and electronic viewpoints in the gas and two solution phases.

In this respect, we first designed an effective structural model for HNTs-T ligand as 1:1 layered alumino silicates and its complex with silver NPs, (displayed in Scheme 1). In the illustrated coordination mode, Ag coordinates to nitrogen of 1,2,3-triazole ring and concurrently can coordinates to oxygen of hydroxyl functional group. It is important to mention that we have shown in our previous research that this size of structural model for an alumino silica supported catalyst has a reliable comport between accuracy and time saving efficiency of computational procedure.

In Figure 8, we have displayed the optimized geometries of HNTs-T ligand and Ag@HNTs-T complex calculated at M06-2X/6-311G** level of theory[50] together with the calculated values of bond order and bond length for Ag-N and Ag-O interactions. It is worthwhile to note that M06-2X has been introduced as a Global hybrid functional with intermediate HF exchange contribution. It is also the top performer within the 06 functional for main group thermochemistry, kinetics and non-covalent interactions. The harmonic frequency analysis was applied to confirm that the found structures correspond to minima.

TABLE 1 Textural property of the Ag@HNTs-T

Catalyst	S_{BET} ($m^2\ g^{-1}$)	Total pore volume ($cm^3\ g^{-1}$)	Average pore diameter (nm)
Ag@HNTs-T	36.2	0.19	21.4
HNTs	51	0.2	15

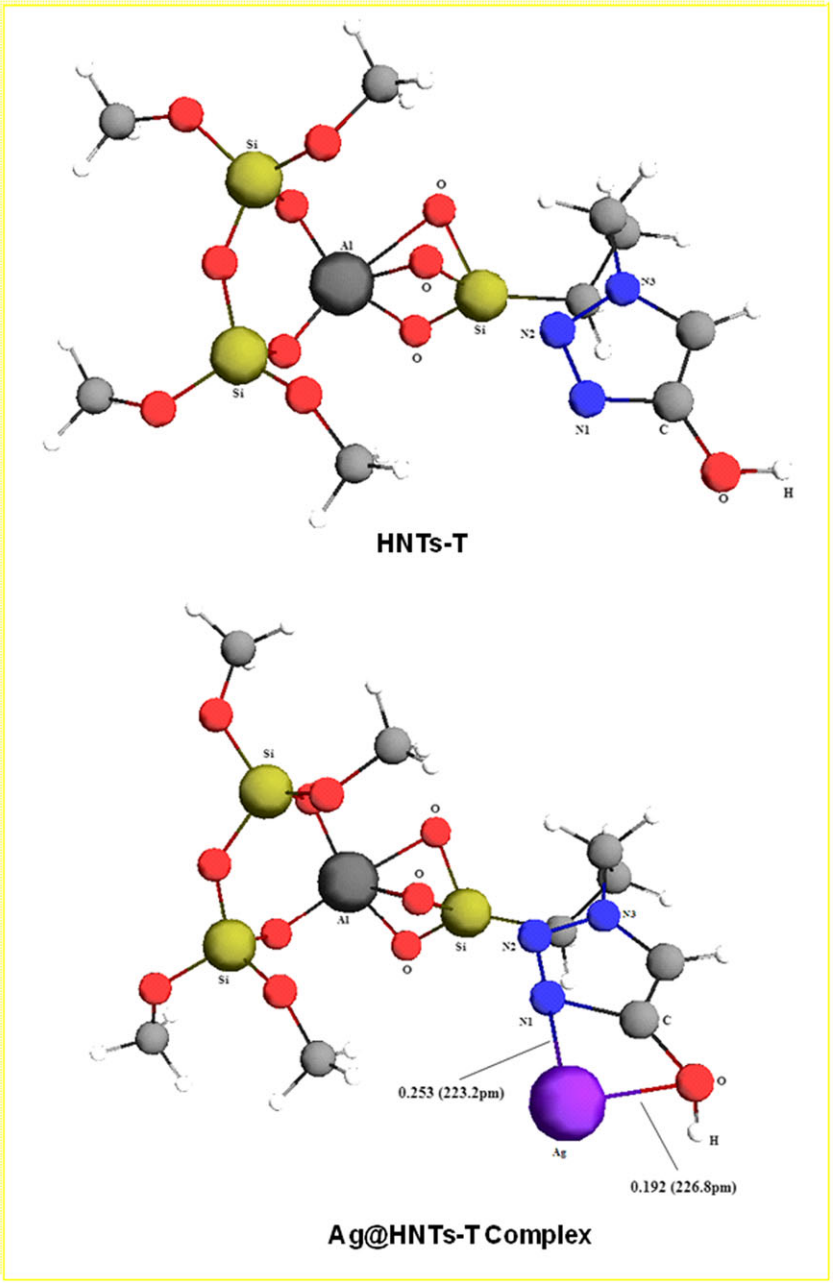

FIGURE 8 The energy-minimized structure of HNTs-T ligand and Ag@HNTs-T complex together with the calculated Ag-O and Ag-N bond orders (bond lengths) obtained at M06-2X/6-311G** level of theory

In the case of silver atom, LANL2TZ effective core potentials (ECPs) were used together with the accompanying basis sets to describe the valence electron density.[51]

Moreover, the solvent effects have been examined from the electronic viewpoint on the basis of a continuum representation of solvent surrounding the substances *via* polarized continuum model.[47] All DFT computations have been performed using GAMESS suite of programs.[52]

To evaluate the variation of bond orders via coordination, we have calculated the bond order and bond length of some key bonds in HNTs-T ligand with their corresponding bonds in Ag@HNTs-T which have been listed in Table 2.

The reported results of Table 2 demonstrate that the calculated values of bond order of C-OH and C-N1 decrease from 1.08 and 1.33 in HNTs-T ligand to 0.83 and 0.98 in Ag@HNTs-T complex indication the coordination of 1*H*-1,2,3-triazole-5-methanol species to the metal. This behavior can be mainly ascribed to the donation of

TABLE 2 The calculated values of some selected bond orders (bond lengths) in HNTs-T ligand and Ag@HNTs-T complex obtained at M06-2X/6-311G** level of theory. Note that numbering of atoms is in accordance with Figure 8

	HNTs-T ligand	Ag@HNTs-T complex
C-OH	1.084 (135.2 pm)	0.835 (142.5 pm)
C-N1	1.339 (135.4 pm)	0.985 (154.1 pm)
O-H	0.939 (96.2 pm)	0.888 (97.4 pm)

shared electrons from this chemical bond to silver atom through the complexation that is further supported with our FT-IR spectroscopic observations. Moreover, comparison of the calculated bond order values of Ag-N and Ag-O in Ag@HNTs-T complex reveals that interaction of silver atom with nitrogen is stronger than the interaction of silver atom with oxygen (0.253 and 0.192 for Ag-N and Ag-O in Ag@HNTs-T complex, respectively.

Precisely speaking, the main bands of the Ag@HNTs-T appeared at 3692 and 3618 cm^{-1} were attributed to O-H and N-H stretching, 1620 cm^{-1} was assigned to C-N stretching and 1365 cm^{-1} was assigned to C-O stretching. Comparatively, the FT-IR spectrum of HNTs-T also shows the main bands around 3692 and 3618 cm^{-1} assigned to O-H and N-H stretching, respectively (as displayed in Figure 5). More importantly, the band at 1637 cm^{-1} attributed to the stretching vibration of the C-N groups has been shifted to 1620 cm^{-1} in the Ag@HNTs-T which can be mainly associated with Ag-HNTs-T interaction. Furthermore, FT-IR spectrum of HNTs-T exhibited a typical band at 1374 cm^{-1} corresponding to the stretching mode of C-O which shifts to the smaller wave numbers (1365 cm^{-1}) after immobilization of Ag NPs in Ag@HNTs-T. Worthy to mention that the similar comparative interpretations between FT-IR bands and calculated metal-ligand interactions are generally considered and reported, previously.[53–56]

In Table 3, we have presented comparatively M06-2X/6-311G** calculated bond orders of Ag-N and Ag-O chemical bonds in the presence of water and toluene as solvents. As it can be seen in Table 3, Ag-N and Ag-O bond orders in Ag@HNTs-T complex has larger calculated values in water solution compared with those obtained in toluene which corroborate the more efficiency of water as solvent rather than toluene. It should be mentioned that effective immobilization and smaller size of silver NPs on functionalized HNTs have been elucidated in water solution in comparison with toluene. [57,58] Finally, we have presented the Highest Occupied Molecular Orbital (HOMO) and the Lowest Unoccupied Molecular Orbital (LUMO) of Ag@HNTs-T complex calculated at M06-2X/6-311G** level of theory (displayed in Figure 9). As we expect from the typical organometallic frontier molecular orbital (FMO) theory,[59] silver neutral atom primarily coordinates to nitrogen and oxygen of ligand through interactions between filled non-bonding orbitals (HOMO) on N and O atoms and an empty dσ orbital (LUMO) on metal atom.

TABLE 3 The obtained values of Ag-O and Ag-N bond orders in Ag@HNTs-T complex complex in water and toluene solution phases, calculated at M06-2X/6-311G** level of theory via PCM approach

	Water	Toluene
Ag-O	0.179	0.158
Ag-N	0.238	0.210

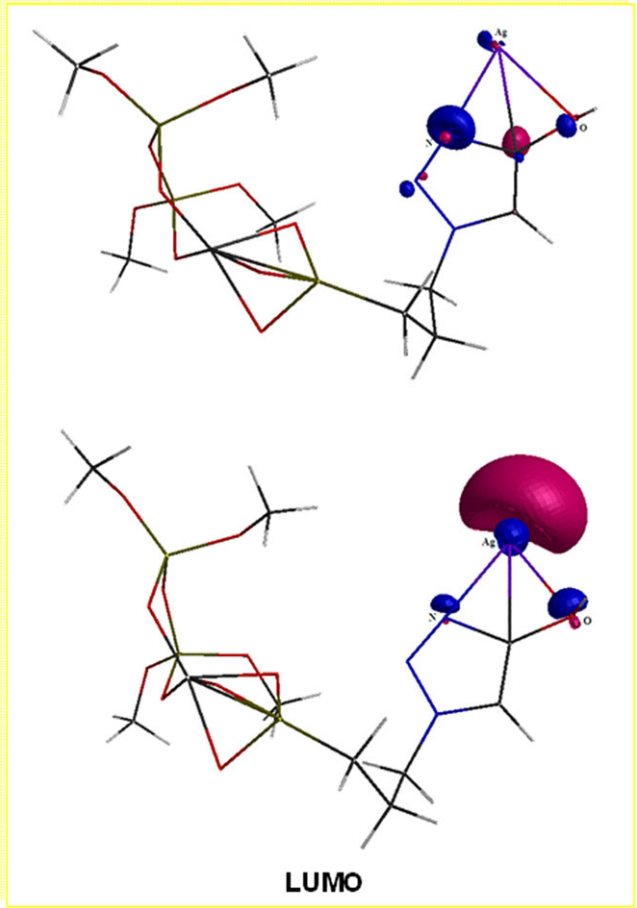

FIGURE 9 Frontier molecular orbital of Ag@HNTs-T complex obtained at M06-2X/6-311G** level of theory

On the basis of these electronic and structural features of Ag@HNTs-T complex, it can be claimed that silver NPs are immobilized on functionalized HNTs majorly at nitrogen of triazole ring sites in the presence of water as preferred solvent.

3.3 | Catalytic activity investigation

In the next step, the catalytic activity of Ag@HNTs-T was investigated. In this line, synthesis of propargylamines through three-component reaction of aldehydes or ketones, amines and acetylenes, A^3 and KA^2 coupling reactions was selected as a chemical transformation. The reason behind this choice was the importance of propargylamines as key intermediates for the synthesis of diverse range of organic compounds with utility for drug industry.

Initially, the reaction of phenyl acetylene, benzaldehyde and morpholine was selected as a model reaction and performed in the presence and absence of the catalyst. It was found that no product was furnished in the absence of the catalyst, indicating the necessity of use of the catalyst

for promoting this reaction. Next, the utility of ultrasonic irradiation for developing an efficient and rapid protocol for this transformation was studied. To this purpose, the model reaction in the presence of 25 mg (1 mol%) of the catalyst was performed in aqueous media under ultrasonic irradiation. The results established that ultrasonic irradiation could promote the reaction rapidly to furnish the desired product in high yield. Notably, the comparison of the efficiency of ultrasonic irradiation with conventional procedures including reflux and stirring condition, proved the superior performance of the former. According to the previous reports, the effect of ultrasonic irradiation can be explained based on the cavitation effect. In other word, ultrasonic irradiation can induce generation, growth and collapse of cavities which can result in the formation of spots with high pressure and temperature.[60]

Confirming the efficiency of the ultrasonic irradiation, the reaction variables including the catalyst amount, reaction solvent and the power of ultrasonic irradiation were optimized by varying these values and studying their effect on the yield of the desired product, Figure 10. As shown in Figure 10, among various solvents used examined for this reaction (toluene, water, ethanol and chloroform), use of water as a solvent resulted in the highest yield of the product. It is also clear that the amount of the catalyst could affect the yield of the desired product. Increasing the amount of the catalyst from 15 to 25 mg significantly improved the yield of the product. However, more increase of this value to 35 mg exerted different effects depending on the ultrasonic power. As obvious in Figure 8, in the case of using ultrasonic power of 120 W increase of the catalyst amount to 35 mg had no effect on the yield of the product while, in the case of using ultrasonic power of 50 W and 100 W, the increase in the catalyst amount led to the increase and decrease of the product yield respectively. Regarding the ultrasonic power, it was found that increasing the power of ultrasonic irradiation from 50 to 100 W positively affected the yield of the product, while further increase of this value had detrimental effect on the yield of the product. This observation can be attributed to the promotion of various side-reactions and formation of by-products as confirmed by GC-MSS analysis. Considering all discussed results, the optimum reaction condition was selected as use of 25 mg of the catalyst, water as solvent and ultrasonic of power 100 W.

Armed with the optimum reaction condition, the generality of this protocol was examined by using various substrates with different steric and electronic properties, Table 4. As tabulated in Table 4, all reactions could be proceed in relatively short reaction times (15-40 min) to afford the corresponding products in high yields. Notably, A^3 coupling reactions were more facile compared to the KA^2 reactions and led to the slightly higher yields in shorter reaction times.

Although the main aim of this research was disclosing the utility of HNTs for developing a novel heterogeneous Ag(0) catalyst and synthesis of propargylamines was selected as a model chemical transformation to establish the catalytic utility of this catalyst, the outstanding efficiency of Ag@HNTs-T, motivated us to study whether using this catalyst under ultrasonic irradiation can be considered as an efficient methodology for these organic reactions. To this purpose, the efficiency of this protocol for the synthesis of the model product was compared with those of Ag NPs, Ag@HNTs and some of previously reported ones (Table 5). Compared to many previously reported catalysts, Table 5, such as Ag^I-Pc-L, Ag-CIN-1, sulfonate-based Cu(I) metal-organic frameworks, Cu(I)MOF, Cu_2O/nano-$CuFe_2O_4$, ZnS, ZnO nano particles and immobilized silver on the

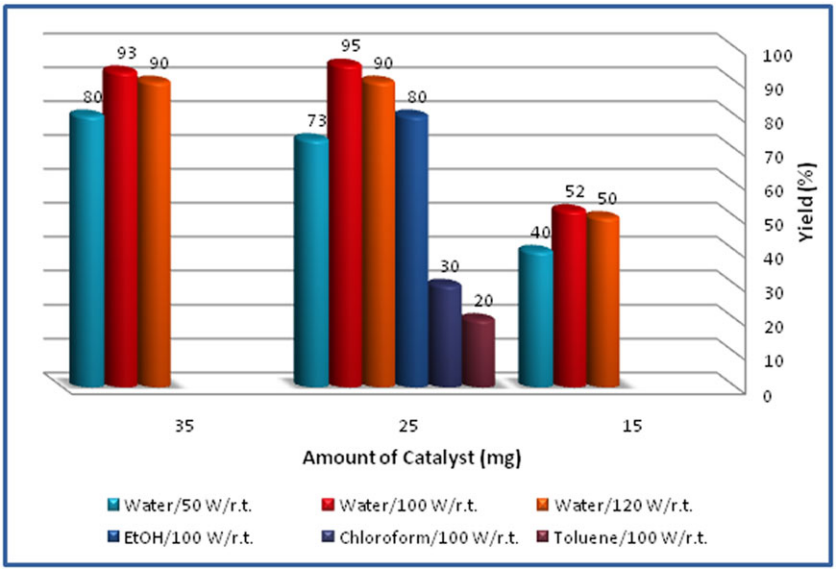

FIGURE 10 Effects of loading of catalyst, duration of reaction and solvent for the synthesis of propargylamine

TABLE 4 Synthesis of three-component reaction of derivatives aldehyde or cyclic ketone, secondary- amines and terminal alkynes catalyzed by Ag@HNTs-T[a] [1,61–66]

R_1	R_2	R_3	R_4	R_5	Product	Time (min)	Yield[b] (%)
1a: C_6H_5	H	4a: -$(CH_2)_5$-		5a: C_6H_5	**6a**	20	90
1b: *p*-Cl-C_6H_4	H	4a		5a	**6b**	18	91
1c: *p*-NO_2-C_6H_4	H	4a		5a	**6c**	20	93
1d: *p*-Me-C_6H_4	H	4a		5a	**6d**	22	89
1e:*p*-MeO-C_6H_4	H	4a		5a	**6e**	15	90
1f:*o*-OH-C_6H_4	H	4a		5a	**6f**	15	90
1 g:Furfuryl	H	4a		5a	**6 g**	20	83
1 h: *p*-$OHCC_6H_4$	H	4a		5a	**6 h**	15	93
1i: *o*-Naphthyl	H	4a		5a	**6i**	18	92
1a	H	4a		5b:*p*-CH_3-C_6H_4	**6j**	22	94
1a	H	4a		5c:*p*-F-C_6H_4	**6 k**	27	85
1a	H	4b:-$(CH_2)_2$-O-$(CH_2)_2$-		5a	**6 l**	17	95
1b	H	4b		5a	**6 m**	20	88
1c	H	4b		5a	**6n**	22	82
1d	H	4b		5a	**6o**	19	90
1e	H	4b		5a	**6p**	17	88
1f	H	4b		5a	**6q**	20	89
1 g	H	4b		5a	**6r**	30	90
1j: *m*-NO_2-C_6H_4	H	4b		5a	**6 s**	30	92
1a	H	4b		5b	**6 t**	20	93
1a	H	4c: -$(CH_2)_4$-		5a	**6u**	22	80
1a	H	4d:C_2H_5	C_2H_5	5a	**6v**	20	92
2a[c]: H	H	4a		5a	**7a**	15	90
2a	H	4a		5b	**7b**	20	85
2a	H	4b		5a	**7c**	22	90
2a	H	4c		5a	**7d**	20	92
2a	H	4d		5a	**7e**	28	82
2b: C_6H_{11}	H	4a		5a	**7f**	18	92
2b	H	4b		5b	**7 g**	27	80
2b	H	4b		5a	**7 h**	19	90
2b	H	4c		5a	**7i**	20	84
2b	H	4d		5a	**7j**	25	80
2c: -$(CH_2)_2$-Me	H	4a		5a	**7 l**	20	90
2c	H	4b		5a	**7 m**	17	85
2c	H	4c		5a	**7n**	25	86
2c	H	4d		5a	**7o**	18	83
3a: -$(CH_2)_4$-		4a		5a	**8a**	30	80
3a		4b		5a	**8b**	35	88
3a		4c		5a	**8c**	37	90
3b: -$(CH_2)_5$-		4a		5a	**8d**	35	92

(Continues)

TABLE 4 (Continued)

R_1	R_2	R_3	R_4	R_5	Product	Time (min)	Yield[b] (%)
3b		4a		5b	**8e**	40	85
3b		4b		5a	**8f**	40	88
3b		4b		5b	**8 g**	40	80
3b		4b		5c	**8 h**	35	82
3b		4c		5a	**8i**	30	88

[a]Reaction conditions: arylaldehydes**1a-j** (1 mmol) or aliphatic aldehyde **2a-c** (1 mmol) or aliphatic ketone **3a, b**(1 mmol), amines **4a-d** (1 mmol), alkynes **5a-c** (1.1 mmol), H_2O (20 ml) and Ag@HNTs-T (0.025 g or 1 mol%) under ultrasonic irradiation (100 W) at room temperature.

[b]Isolated yield.

[c]Aqueous formaldehyde (37%, 0.4 ml).

TABLE 5 Comparison of Ag@HNTs-T with other recently reported metal catalysts for the synthesis of propargylamine[a]

Entry	Catalyst	Reaction conditions	Time (min)	Catalyst amount	Yield[b] (%)	Ref
1	Ag@HNTs-T	H_2O / r.t./US	17	25 mg (1 mol%)	95	This work
2	h-Fe_2O_3@DA/Ag	S.F./ 90 °C	60	10 mg	96	[66]
3	h-Fe_2O_3@SiO_2-CD/Ag	H_2O/ r.t./ US	8	20 mg	97	[23]
4	ZnO nano particles	Stirrer/ 90 °C	120	10 mol%	89	[67]
5	Immobilized Silver on Surface-modified ZnO NPs	Reflux/ H_2O	240	10 mol%	89	[68]
6	Ag-CIN-1[c]	H_2O/ 40 °C	720	5 mg	65	[4]
7	Ag^I-Pc-L[d]	Toluene/MW/ 150 °C	20	3 mol%	59	[69]
8	CuNPs/TiO_2	Neat/ 70 °C	420	0.5 mol%	91	[70]
9	ZnS	Reflux/ CH_3CN	270	10 mol%	89	[71]
10	sulfonate-based Cu(I) metal-organic frameworks	Reflux/EtOH, 90 °C	1440	20 mg	87	[72]
11	CuI catalysts supported on protonated trititanate nanotubes	Solvent-free, 70 °C	90	20 mg	95	[73]
12	Cu_2O/nano-$CuFe_2O_4$	Solvent-free, 90 °C	40	10 mg	93	[74]
13	Cu(I)MOF	Neat/ 80 °C	60	2.5 mol%	90	[72]
14	CuI@HNTs-2 N	EtOH/ r.t./ US	10	30 mg	95	[29]
15	Cu@Fur-SBA-15	Solvent-free/ r.t.	15	0.5 mol%	95	[27]
16	Ag	H_2O / r.t./US	17	25 mg	40	This work
17	Ag@HNTs	H_2O / r.t./US	17	25 mg	75	This work

[a]Reaction conditions: morpholine (1 mmol), benzaldehyde (1 mmol), phenylacetylene (1.1 mmol) in the presence of different conditions.

[b]Isolated yield.

[c]Ag-grafted covalent imine network material.

[d]Ag(I)(Pyridine-Containing Ligand) Complexes.

[e]Cu(II) immobilized on aminatedepichlorohydrin activated silica.

[f]benzylated MCM-41 solfunic acid.

surface-modified ZnO nanoparticles, Ag@HNTs-T exhibited superior catalytic activity and furnished the desired product in higher yields. Some other catalysts such as Cu@Fur-SBA-15, CuI@HNTs-2 N, CuI catalysts supported on protonated trititanate nanotubes, h-Fe_2O_3@DA/Ag, however, exhibited comparative or slightly higher catalytic activity compared to Ag@HNTs-T.

Comparison of the efficiency of Ag@HNTs-T with those of Ag NPs, Ag@HNTs proved the higher catalytic activity of the former. According to the previous reports, the role of HNT can be described in terms of improvement

of the distribution of Ag nanoparticles and reducing their sizes.[10]

On the other hand, the functionalities on the surface of HNTs plays an important role in anchoring Ag(0) nanoparticles and reducing the leaching (as the ICP results confirmed).

3.4 | Reaction mechanism

The plausible reaction mechanism for the synthesis of propargylamines is depicted in Scheme 2. According to the previous reports[63,66] the reaction initiated by the activation of the terminal C-H bond of acetylene by silver nanoparticles immobilized on the functionalized HNT and production of an intermediate. The latter then reacted with imnium ion obtained from the condensation reaction of aldehyde or ketone and amine to furnish the corresponding propargylamine derivative and Ag@HNTs-T catalyst.

3.5 | Recyclability of the catalyst

Considering the importance of the recyclability of the heterogeneous catalyst from the industrial and economical points of view and to elucidate whether the immobilization of silver nanoparticles was efficiently carried out on the functionalized HNTs, the recyclability of Ag@HNTs-T was investigated for ten cycles. To the purpose, the yield of the model product in the presence of the fresh Ag@HNTs-T was compared with those of recycled catalysts. In this line, the recovered catalyst was washed with EtOH, dried at 100 °C for 8 h and recycled for consecutive reaction runs. The results of the recyclability experiments are depicted in Figure 11. As shown in Figure 11, the catalyst could be recovered and recycled for ten reaction runs with slight loss of the catalytic activity, observed. Notably, recycling of the catalyst for ten reactions run led to the significant decrease in the yield of the product of model reaction (the product was obtained in 78% yield).

To investigate the reason behind this observation, the leaching of silver nanoparticles was studied by using ICP-AES. The obtained results indicated the heterogeneous nature of the catalyst. The results demonstrated that the leaching of Ag(0) nanoparticles for the recycled catalyst for ten reactions run was only 0.0032 %w/w, while this value for the recycled catalyst for tenth reaction run was significant.

3.6 | Spectral data for some selected compounds, supporting information

3.6.1 | 1-(1,3-diphenylprop-2-ynyl)piperidine (Table 4, 6a)

Pale yellow oily liquid; ^{1}H NMR (400 MHz, $CDCl_3$, ppm) δ 1.45-1.49 (m, 2H), 1.58-1.65 (m, 4H), 2.59 (t, 4H), 4.81 (s, 1H), 7.31-7.40 (m, 6H), 7.53-7.55 (m, 2H), 7.65-67 (d, *J*=7.6 Hz, 2H).

3.6.2 | 1-(3-phenyl-1-(4-(3-phenyl-1-(piperidin-1-yl)prop-2-ynyl)phenyl)prop-2-ynyl)piperidine (Table 4, 6 h)

White solid; mp 157-159 °C (Lit.[66] 158-160 °C); ^{1}H NMR (400 MHz, $CDCl_3$, ppm) δ 1.47 (m, 2H), 1.59-1.63 (m, 4H),

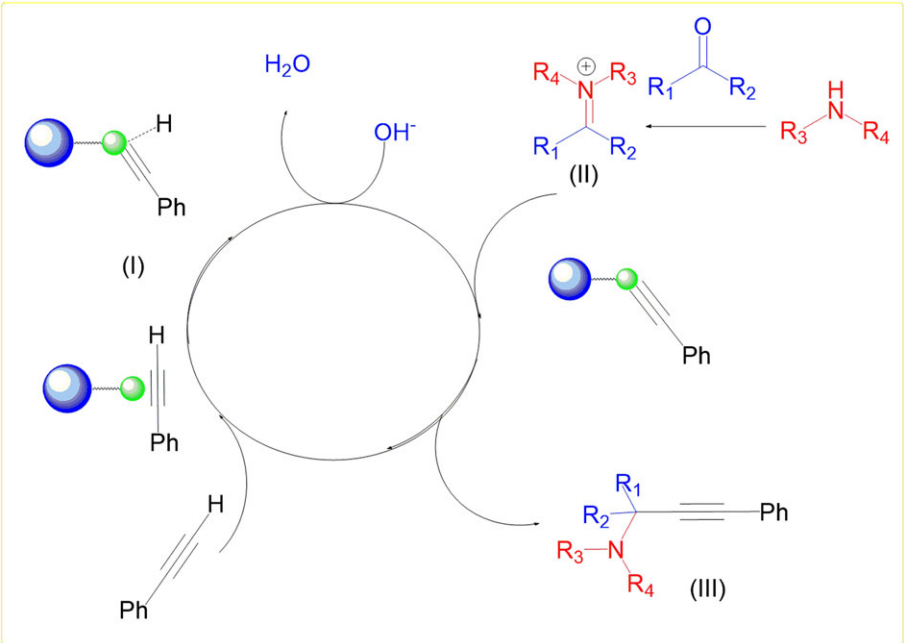

SCHEME 2 The plausible mechanism for the synthesis of propargylamine under the Ag@HNTs-T catalysis

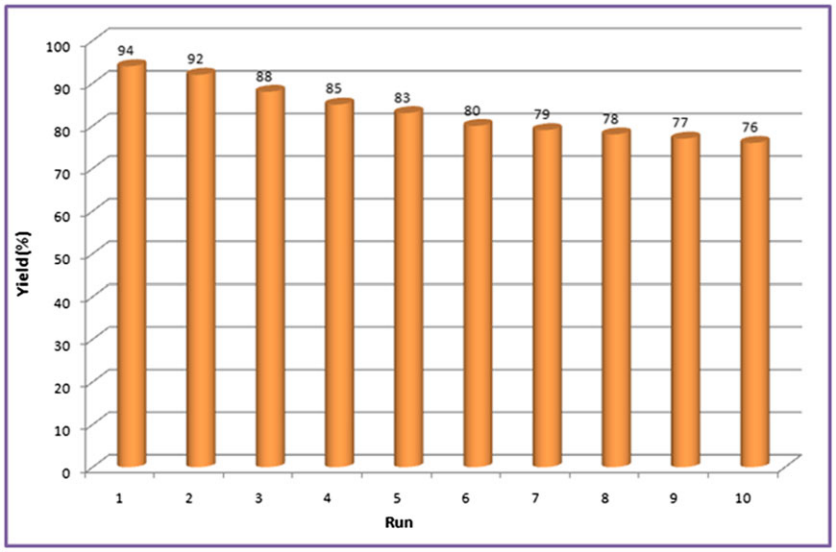

FIGURE 11 The recyclability of the catalyst

2.59 (m, 4H), 4.81 (s, 1H), 7.33-7.35 (m, 3H), 7.52-7.55 (m, 2H), 7.63 (s, 2H).

3.6.3 | 1-(1-(naphthalen-3-yl)-3-phenylprop-2-ynyl)piperidine (Table 4, 6i)

Yellow oil; ^{1}H NMR (400 MHz, $CDCl_3$, ppm): δ 1.47-1.51 (m, 2H), 1.60-1.67 (m, 4H), 2.64 (t, 4H), 4.97 (s, 1H), 7.36-7.40 (m, 3H), 7.48-7.52 (m, 2H), 7.58-7.61 (m, 2H), 7.79 (dd, J^1=J^2= 8.4 Hz, 1H), 7.85-7.91 (m, 3H), 8.11 (s, 1H); ^{13}C NMR (100 MHz, $CDCl_3$, ppm) d 24.4, 26.2, 50.8, 62.5, 86, 88.1, 123.3, 125.8, 125.9, 126.7, 127.2, 127.5, 127.7, 128.1, 128.12, 131.8, 132.9, 133.1, 136.3.

3.6.4 | N,N-diethyl-1,3-diphenylprop-2-yn-1-amine (Table 4, 6v)

Pale yellow oily liquid; ^{1}H NMR (400 MHz, $CDCl_3$, ppm) δ 1.04 (m, 6H), 2.36-2.62 (m, 4H), 5.19 (s, 1H), 7.15-7.27 (m, 4H), 7.29-7.38 (m, 3H), 7.39-7.41 (m, 2H).

3.6.5 | 4-(3-phenylprop-2-ynyl)morpholine (Table 4, 7c)

Yellow oil; ^{1}H NMR (400 MHz, $CDCl_3$, ppm) δ 2.64-2,67 (m, 6H), 3.52 (s, 3H), 3.69-3.71 (m, 1H), 3.77-3.79 (m, 6H), 7.28-7.31 (m, 4H), 7.43-7.46 (m, 2H).

3.6.6 | 1-(1-cyclohexyl-3-phenylprop-2-ynyl)pyrrolidine (Table 4, 7i)

Colorless liquid; ^{1}H NMR (400 MHz, $CDCl_3$, ppm) δ 1.05-1.36 (m, 5H), 1.56-1.63 (m, 2H), 1.75-1.79 (m, 6H), 1.82-2.10 (m, 4H), 2.5-2.98 (m, 4H), 3.36-3.38 (d, J =7.6 Hz, 1H), 7.14-7.33 (m, 3H), 7.50-7.63 (m, 2H). ^{13}C NMR (100 MHz, $CDCl_3$, ppm) δ 24.9, 26.9, 27.1, 28.3, 32.7, 33, 42.9, 51.1, 61.1, 86.1, 88.9, 125.9, 128.9, 129.8, 132.6.

3.6.7 | 4-(1-phenylhex-1-yn-3-yl) morpholine (Table 4, 7 m)

Yellow oil; ^{1}H NMR (400 MHz, DMSO-d_6, ppm) δ 0.97 (m, 3H), 1.45-1.75 (m, 4H), 2.67−2.70 (m, 2H), 2.79−2.83 (m, 2H), 3.82-4.13 (m, 1H), 4.15-4.17 (m, 4H), 7.46−7.50 (m, 3H), 7.62−7.64 (m, 2H).

3.6.8 | 4-(1-(2-phenylethynyl)cyclohexyl) morpholine (Table 2, 8f)

Pale yellow oily liquid; ^{1}H NMR (400 MHz, $CDCl_3$, ppm) δ 1.28-1.30 (m, 1H), 1.52 (m, 2H), 1.63-1.67 (m, 3H), 1.73 (br.s, 2H), 2.03-2.05 (m, 2H), 2.74 (br.s, 4H), 3.78 (br.s, 4H), 7.27 (m, 3H), 7.44-7.45 (m, 2H), ^{13}C NMR (100 MHz, $CDCl_3$, ppm) δ 22.7, 25.7, 35.4, 46.6, 58.8, 67.4, 86.4, 89.8, 123.4, 127.7, 128.1, 131.7.

3.6.9 | 4-(1-((4-fluorophenyl)ethynyl) cyclohexyl)morpholine (Table 4, 8 h)

Yellow oil; ^{1}H NMR (400 MHz, DMSO-d_6, ppm) δ 1.26-1.34 (m, 1H), 1.57-1.62 (m, 2H), 1.69-1.78 (m, 3H), 1.80-1.86 (m, 2H), 2.00-2.02 (m, 2H), 2.78 (s, 4H), 3.70 (br.t, J = 4.2 Hz, 4H), 6.97-7.00 (t, J = 8.6 Hz, 2H), 7.32-7.40 (m, 2H).

4 | CONCLUSION

In summary, HNTs was successfully functionalized with 1*H*-1,2,3-triazole-5-methanol and used as a support for immobilization of silver nanoparticles and developing a

novel catalyst, Ag@HNTs-T. The reduction of silver salt and capping of Ag(0) nanoparticles were achieved by using a bio-assisted approach using Arctiumplatylepis extract. The catalytic activity of the catalyst was examined for A^3 and KA^2 coupling reactions. The results established that Ag@HNTs-T could efficiently promote these reactions under ultrasonic irradiation to furnish the corresponding products in high yields. Noteworthy, the catalyst was recyclable up to ten reaction runs and the silver leaching was dramatically suppressed. Moreover, our DFT and PCM computational results are in confirmation with the experimental observations for the nanocatalyst from the structural and electronic viewpoints.

ACKNOWLEDGEMENTS

The authors appreciate partial financial supports from Alzahra University and Iran Polymer and Petrochemical Institute. MMH is also thankful to Iran National Science Foundation (INSF) for the given individual research chair.

ORCID

Majid M. Heravi http://orcid.org/0000-0003-2978-1157
Samahe Sadjadi http://orcid.org/0000-0002-6884-4328

REFERENCES

[1] S. V. Katkar, R. V. Jayaram, *RSC Adv.* **2014**, *4*, 47958.

[2] B. J. Borah, S. J. Borah, K. L. Saikia, D. K. Dutta, *Catal. Sci. Technol.* **2014**, *4*, 4001.

[3] T. Zeng, W.-W. Chen, C. M. Cirtiu, A. Moores, G. Song, C.-J. Li, *Green Chem.* **2010**, *12*, 570.

[4] N. Salam, S. K. Kundu, R. Ali Molla, P. Mondal, A. Bhaumik, S. Manirul Islam, *RSC Adv.* **2014**, *4*, 47593.

[5] H. Naeimi, M. Moradian, *Appl. Organometal. Chem.* **2013**, *27*, 300.

[6] N. Salam, S. K. Kundu, A. Singha Roy, P. Mondal, S. Roy, A. Bhaumik, S. Manirul Islam, *Catal. Sci. Technol.* **2013**, *3*, 3303.

[7] G. Villaverde, A. Corma, M. Iglesias, F. Sanchez, *ACS Catal.* **2012**, *2*, 399.

[8] L. F. Bobadilla, T. Blasco, J. A. Odriozola, *Phys. Chem. Chem. Phys.* **2013**, *15*, 16927.

[9] M. Hosseini-Sarvari, F. Moeini, *New J. Chem.* **2014**, *38*, 624.

[10] M. Massaro, C. G. Colletti, G. Lazzara, S. Milioto, R. Noto, S. Riela, *J. Mater. Chem. A* **2017**, *5*, 13276.

[11] P. Yuan, P. D. Southon, Z. Liu, M. E. R. Green, J. M. Hook, S. J. Antill, C. J. Kepert, *J. Phys. Chem. C* **2008**, *112*, 15742.

[12] S. Barrientos-Ramírez, E. V. Ramos-Fernández, J. Silvestre-Albero, A. Sepúlveda-Escribano, M. M. Pastor-Blas, A. González-Montiel, *Microporous Mesoporous Mater.* **2009**, *120*, 132.

[13] Y. Zhang, H. Yang, *Phys. Chem. Miner.* **2012**, *39*, 789.

[14] Y. Zhang, J. Ouyang, H. Yang, *Appl. Clay Scie.* **2014**, *95*, 252.

[15] R. S. Murali, M. Padaki, T. Matsuura, M. S. Abdullah, A. F. Ismail, *Sep.Purif.Technol.* **2014**, *132*, 187.

[16] Y. Zhang, A. Tang, H. Yang, J. Ouyang, *Appl. Clay Sci.* **2016**, *119*, 8.

[17] M. Massaro, V. Schembri, V. Campisciano, G. Cavallaro, G. Lazzara, S. Milioto, R. Noto, F. Parisi, S. Riela, *RSC Adv.* **2016**, *6*, 55312.

[18] M. Massaro, S. Riela, G. Cavallaro, C. G. Colletti, S. Milioto, R. Noto, F. Parisi, G. Lazzara, *J. Mol. Catal. A.* **2015**, *408*, 12.

[19] M. Massaro, S. Riela, G. Lazzara, M. Gruttadauria, S. Milioto, R. Noto, *Appl. Organomet. Chem.* **2014**, *28*, 234.

[20] V. A. Vinokurov, A. V. Stavitskaya, Y. A. Chudakov, E. V. Ivanov, L. K. Shrestha, K. Ariga, Y. A. Darrat, Y. M. Lvov, *Sci. Technol. Adv. Mater.* **2017**, *18*, 147.

[21] S. Battistoni, A. Dimonte, E. Ubaldi, Y. Lvov, V. Erokhin, *J. Nanosci. Nanotechnol.* **2017**, *17*, 5310.

[22] R. Noto, S. Milioto, G. Lazzara, M. Massaro, S. Riela, *J. Mater. Chem. B* **2017**, *5*, 2867.

[23] S. Sadjadi, M. Malmir, M. M. Heravi, *RSC Adv.* **2017**, *7*, 36807.

[24] S. Sadjadi, M. M. Heravi, *RSC Adv.* **2016**, *6*, 88588.

[25] S. Sadjadi, M. M. Heravi, M. Daraie, *J. Mol. Liq.* **2017**, *231*, 98.

[26] S. Sadjadi, M. M. Heravi, *Res. Chem. Intermed.* **2017**, *43*, 2201.

[27] S. Sadjadi, M. M. Heravi, *RSC Adv.* **2017**, *7*, 30815.

[28] S. Sadjadi, M. M. Heravib, M. Malmir, B. Masoumi, *Appl. Organomet. Chem.* .

[29] S. Sadjadi, N. Bahri-Laleh, *J. Porous Mater.* **2017**, In press.

[30] M. M. Heravi, M. Tamimi, H. Yahyavi, T. Hosseinnejad, *Curr. Org. Chem.* **2016**, *20*, 1591.

[31] T. Hosseinnejad, B. Fattahi, M. M. Heravi, *J. Mol. Modeling* **2015**, *21*, 264.

[32] F. Ebrahimpour-Malamir, T. Hosseinnejad, R. Mirsafaei, M. M. Heravi, *Appl. Organomet. Chem.* **2017**, e3913.

[33] T. Baie Lashaki, H. A. Oskooie, T. Hosseinnejad, M. M. Heravi, *J. Coord. Chem.* **2017**, *70*, 1815.

[34] T. Hossiennejad, M. Daraie, M. M. Heravi, N. N. Tajoddin, *J. Inorg. Organomet. Polym.* **2017**, *27*, 861.

[35] M. M. Heravi, T. Hosseinnejad, N. Nazari, *Can. J. Chem.* **2017**, *95*, 530.

[36] T. Hosseinnejad, T. Kazemi, *Mol. Cryst. Liq. Cryst.* **2016**, *637*, 53.

[37] R. Mirsafaei, M. M. Heravi, T. Hosseinnejad, S. Ahmadi, *Appl. Organomet. Chem.* **2016**, *30*, 823.

[38] V. Zadsirjan, M. M. Heravi, M. Tajbakhsh, H. A. Oskooie, M. Shiri, T. Hosseinnejad, *Res. Chem. Inter.* **2016**, *42*, 6407.

[39] R. Mirsafaei, M. M. Heravi, S. Ahmadi, T. Hosseinnejad, *Chem. Pap.* **2016**, *70*, 418.

[40] R. Mirsafaei, M. M. Heravi, S. Ahmadi, M. H. Moslemin, T. Hosseinnejad, *J. Mol. Catal. A: Chem.* **2015**, *402*, 100.

[41] S. Khaghaninejad, M. M. Heravi, T. Hosseinnejad, H. A. Oskooie, M. Bakavoli, *Res. Chem. Intermed.* **2016**, *42*, 1593.

[42] W. O. Yah, H. Xu, H. Soejima, W. Ma, Y. Lvov, A. Takahara, *J. Am. Chem. Soc.* **2012**, *134*, 12134.

[43] F. Yu, H. Deng, H. Bai, Q. Zhang, K. Wang, F. Chen, Q. Fu, *ACS Appl. Mater. Interfaces* **2015**, *7*, 10178.

[44] M. C. Da Silva, E. C. Dos Santos, M. P. Lourenço, H. A. Duarte, *J. Mol. Model.* **2013**, *19*, 1995.

[45] R. Demichelis, Y. Noel, P. D'arco, L. Maschio, R. Orlando, R. Dovesi, *J. Mater. Chem.* **2010**, *20*, 10417.

[46] C. Lee, W. Yang, R. G. Parr, *Phys. Rev. B* **1988**, *37*, 785.

[47] V. Barone, M. Cossi, *J. Phys. Chem. A.* **1998**, *102*, 1995.

[48] H. Zhu, M. L. Du, M. L. Zou, C. S. Xu, Y. Q. Fu, *Dalton Trans.* **2012**, *41*, 10465.

[49] A. D. Becke, *J. Chem. Phys.* **1993**, *98*, 1372.

[50] Y. Zhao, D. G. Truhlar, *Theor. Chem. Acc.* **2008**, *120*, 215.

[51] P. J. Hay, W. R. Wadt, *J. Chem. Phys.* **1985**, *82*, 270.

[52] M. W. Schmidt, K. K. Baldridge, J. A. Boatz, S. T. Elbert, M. S. Gordon, J. H. Jensen, S. Koseki, N. Matsunaga, K. A. Nguyen, S. Su, T. L. Windus, M. Dupuis, J. A. Montgomery, *J. Comput. Chem.* **1993**, *14*, 1347.

[53] A. R. Chowdhuri, S. Tripathy, C. Haldar, S. Chandra, B. Das, S. Roy, S. K. Sahu, *RCS Adv.* **2015**, *5*, 21515.

[54] H. Kumar, R. Rani, *IJESIT* **2013**, *3*, 344.

[55] C. Dablemont, P. Lang, C. Mangeney, J.-Y. Piquemal, V. Petkov, F. Herbst, G. Viau, *Langmuir* **2008**, *24*, 5832.

[56] S. Sadjadi, T. Hosseinnejad, M. Malmir, M. M. Heravi, *New J. Chem.* **2017**, *41*, 13935.

[57] J. Mondal, A. Modak, A. Dutta, S. Basu, S. N. Jha, D. Bhattacharyya, A. Bhaumik, *Chem. Commun.* **2012**, *48*, 8000.

[58] J. Mondal, A. Modak, A. Dutta, A. Bhaumik, *Dalton Trans.* **2011**, *40*, 5228.

[59] I. Fleming, London: Wiley **1978**, pp. 29.

[60] S. Sadjadi, M. Eskandari, *Ultrason. Sonochem.* **2013**, *20*, 640.

[61] M. S. Hosseini, F. Moeini, *New J. Chem.* **2014**, *38*, 624.

[62] M. Tajbaksh, M. Farhang, H. R. Mardani, R. Hosseinzadeh, Y. Sarrafi, *Chin. J. Cat.* **2013**, *34*, 2217.

[63] L. Shi, Y.-Q. Tu, M. Wang, F.-M. Zhang, C.-A. Fan, *Org. Lett.* **2004**, *6*, 1001.

[64] J. Safaei-Ghomi, M. A. Ghasemzadeh, A. Kakavand-Qalenoei, J. Saudi, *Chem. Soc.* **2016**, *20*, 502.

[65] M. Tajbakhsh, M. Farhang, M. Baghbanian, H. Hosseinzadeh, M. Tajbakhsh, *New J. Chem.* **2015**, *39*, 1827.

[66] A. Elhampour, M. Malmir, E. Kowsari, F. A. Boorboor, F. Nemati, *RSC Adv.* **2016**, *6*, 96623.

[67] K. V. V. Satyanarayana, P. Atchuta Ramaiah, Y. L. N. Murty, M. R. Chandra, S. V. N. Pammi, *Catalysis Commun.* **2012**, *25*, 50.

[68] F. Movahedia, H. Masrouria, M. Z. Kassaee, *J. Mol. Catal. A.* **2014**, *395*, 52.

[69] M. Trose, M. Dell'Acqua, T. Pedrazzini, V. Pirovano, E. Gallo, E. Rossi, A. Caselli, G. Abbiati, *J. Org. Chem.* **2014**, *79*, 7311.

[70] M. J. Albaladejo, F. Alonso, Y. Moglie, M. Yus, *Eur. J. Org. Chem.* **2012**, *2012*, 3093.

[71] N. P. Eagalapati, A. Rajack, Y. L. N. Murthy, *J. Mol. Catal. A.* **2014**, *381*, 126.

[72] P. Li, S. Regati, H.-C. Huang, H. D. Arman, B.-L. Chen, J. C.-G. Zhao, *Chin. Chem. Lett.* **2015**, *26*, 6.

[73] B. R. Prasad Reddy, P. V. Govardhana Reddy, M. V. Shankar, B. N. Reddy, *Asian J. Org. Chem.* **2017**, *6*, 712.

[74] F. Nemati, A. Elhampour, H. Farrokhi, M. Bagheri Natanzi, *Catal. Commun.* **2015**, *66*, 15.

SUPPORTING INFORMATION

Additional Supporting Information may be found online in the supporting information tab for this article.

How to cite this article: Malmir M, Heravi MM, Sadjadi S, Hosseinnejad T. Ultrasonic and bio-assisted synthesis of Ag@HNTs-T as a novel heterogeneous catalyst for the green synthesis of propargylamines: A combination of experimental and computational study. *Appl Organometal Chem*. 2018;e4291. https://doi.org/10.1002/aoc.4291